Research Square

Preprints are preliminary reports that have not undergone peer review.
They should not be considered conclusive, used to inform clinical practice,
or referenced by the media as validated information.

Impedance Matrix Analysis of Transformer Winding Resonances with Different Insulation Media

Irene Woyna

irene.woyna@hitachienergy.com

Hitachi Energy Germany AG

Ali Al-Abadi

Hitachi Energy Germany AG

Digpalsinh Parmar

Hitachi Energy India Limited

Research Article

Keywords: Transformer insulation, transformer winding resonance, transient overvoltages

Posted Date: July 20th, 2026

DOI: https://doi.org/10.21203/rs.3.rs-10207952/v1

License: This work is licensed under a Creative Commons Attribution 4.0 International License.
Read Full License

Additional Declarations: No competing interests reported.

Impedance Matrix Analysis of Transformer Winding Resonances with Different Insulation Media

Irene Woyna[1], Ali Al-Abadi[1] and Digpalsinh Parmar[2]
[1]Hitachi Energy AG, Germany
[2]Hitachi Energy India Limited, India
E-mail: irene.woyna@hitachienergy.com

Abstract – This paper presents a finite element based methodology for deriving frequency dependent impedance matrices of transformer windings and for analysing their resonance behaviour in relation to different insulation systems. By comparing dry, mineral oil immersed, and retrofilled natural ester insulation in a 630 kVA layer-wound HV winding, the study demonstrates how the dielectric properties of the insulation medium influence capacitive coupling, resonance damping, and internal voltage stress within an Frequency Response Analysis (FRA) framework.

Keywords: Transformer insulation, transformer winding resonance, transient overvoltages.

1. Introduction

Modern power systems increasingly expose transformers to very fast transient overvoltages (VFTO) generated by lightning, switching operations, line and capacitor-bank energization, power-electronic converters, and the expanded use of Gas Insulated Switchgear (GIS). GIS disconnectors can produce nanosecond-scale, ultra-steep fronts with significant high-frequency content. These fast transients launch travelling waves into the transformer terminals, driving high-frequency components deep into the winding structure.

Inside the winding, the voltage does not distribute uniformly. Instead, it concentrates near the end line, across the first turns or disks, especially when the surge front is steep. This localized electrical stress can initiate partial discharge, accelerate insulation aging, and, under severe resonance conditions, lead to dielectric breakdown. The challenge is amplified further by the trend toward compact transformer designs with reduced insulation margins, which improves efficiency but increases sensitivity to VFTO and high-frequency resonances.

Standards such as IEC 60076-3 define lightning impulse (LI) and switching impulse (SI) test requirements; however, these waveforms do not fully represent VFTO, which include repeated sub-microsecond fronts and a much broader frequency spectrum. Several studies show that realistic transient excitation combined with wide-band transformer models is needed to accurately predict internal stresses on turns, coils, and sections [1], [4], [5].

To capture wide-band behaviour, engineers typically employ RLCG ladder models, where each node represents a turn, disk, or section, and the interconnections represent inductive, capacitive, and dielectric couplings. Accuracy depends strongly on how the parameters of the model are obtained. Classical analytical formulations, such as those introduced in [7], remain essential for deriving self and mutual impedances and performing sensitivity studies. More recent work has demonstrated the benefits of impedance-matrix formulations, as introduced by [2], which allow direct identification of natural frequencies, amplification factors, and overvoltage hotspots. Complementary research using finite element methods (FEM) provides frequency-dependent inductances, capacitances, and losses, and quantifies the influence of core properties and mechanical displacements on the frequency response [3], thereby improving both ladder models [9] and the interpretation of Frequency Response Analysis (FRA) measurements [6], [10].

Transformer winding resonance behaviour is strongly influenced by insulation properties through their impact on capacitive coupling and dielectric losses. In this study, a step-down 630 kVA power transformer is investigated with a focus on the high-voltage (HV) layer-wound winding, which is particularly sensitive to dielectric configuration and high-frequency phenomena. Three insulation scenarios are considered – dry insulation, mineral oil impregnation, and natural ester impregnation – representing different combinations of relative permittivity and dissipation factors. The objective is to quantify how these insulation systems modify the winding impedance matrix and, consequently, its

frequency response and resonance characteristics.

A frequency-domain finite element modelling approach is employed to derive the impedance and admittance matrices of the HV winding. A 2D axisymmetric model captures the dominant electromagnetic interactions while maintaining computational efficiency. The analysis spans a wide frequency range relevant to both power-frequency operation and FRA. By combining electro- and magneto-quasistatic formulations and incorporating frequency-dependent material properties, the resulting impedance matrices provide a physically consistent basis for resonance analysis, insulation condition assessment, and interpretation of dielectric effects in transformer windings.

2. Model Description and Impedance Matrix Extraction

In this study, a step-down 630 kVA, 30/0.4 kV power transformer is investigated, with particular emphasis on the high-voltage (HV) layer-wound winding, which is known to be highly sensitive to dielectric properties and resonance phenomena. The objective is to quantify how different insulation systems influence the winding impedance matrix and its resulting frequency response. Three insulation scenarios are considered, as summarized in Table I, representing dry insulation, conventional mineral-oil impregnation, and natural-ester impregnation after a retrofill. These scenarios differ in both relative permittivity and dielectric loss tangent of the solid and liquid insulation, thereby allowing a systematic investigation of capacitive coupling enhancement and dielectric damping effects.

Table 1. Insulator material properties: OIP Oil-impregnated kraft paper, EIP Ester impregnated Kraft paper. MO mineral oil, NE natural ester.

Scenario	Solid	ε_r	$\tan\delta$	Liquid	ε_r	$\tan\delta$
1	Dry	3	0.2	N/A	1	0
2	OIP	3.9	0.55	MO	2.2	0.1
3	EIP	4.2	0.8	NE	3.2	0.3

A 2D axisymmetric finite-element model of the HV winding was developed to capture the dominant electromagnetic interactions within the winding structure as shown in Figure 1. The model includes detailed representations of conductors, solid insulation, and surrounding liquid insulation, while exploiting axial symmetry to reduce computational cost without compromising physical fidelity. The winding was analysed using frequency-domain solvers over a range from 50Hz to 300kHz, discretised into 96 logarithmically spaced frequency points. This range covers both power frequency behaviour and higher frequency resonances relevant to VFTO.



Fig. 1. Close-up of the 2D axisymmetrical winding model used in the time-harmonic electric FEM simulation. Blue color denotes the liquid insulator, grey solid insulator, and black conductor- the detailed description of the considered scenarios and material parameters are given in Table 1. Symmetry axis here is aligned with horizontal orientation.

Frequency dependent material behaviour was incorporated by modelling the dielectric losses via the dissipation factor $\tan\delta$ and the magnetic core via a frequency-dependent relative permeability $\mu_r(\omega)$.

The electric field problem was solved using an electro-quasistatic AC conduction formulation, which computes the scalar electric potential ϕ by simultaneously accounting for conduction and displacement currents. The governing equation is given by

$$\nabla \cdot [(\sigma + j\omega\varepsilon_0\varepsilon_r)\nabla\phi] = 0 \tag{1}$$

where ε_r is the complex relative permittivity

$$\varepsilon_r = \varepsilon_r' - j\varepsilon_r'' \tag{2}$$

and the dissipation factor is defined as:

$$\tan\delta = \frac{\varepsilon_r''}{\varepsilon_r'} \approx \frac{\sigma}{\omega\varepsilon_0}, \tag{3}$$

where σ is the electrical conductivity of the insulator and ε_0 vacuum permittivity.

In this formulation, the real part of the permittivity governs electric energy storage and capacitive coupling, while the imaginary part introduces dielectric losses. Consequently, increasing ε_r primarily enhances the imaginary (reactive) component of the admittance matrix by strengthening

electric field coupling between winding layers, whereas increasing $\tan\delta$ increases the real (dissipative) component, providing damping that reduces resonance amplitudes without significantly shifting resonance frequencies.

The magnetic field problem was solved using a magneto-quasistatic frequency-domain formulation based on the magnetic vector potential $\mathbf{A}$:

$$\nabla \times \left(\frac{1}{\mu}\nabla \times \mathbf{A}\right) + j\omega\sigma\mathbf{A} = \mathbf{J}_s, \quad (4)$$

where μ is permeability, σ electrical conductivity, and $\mathbf{J}_s$ source current. The equation captures inductive coupling through the magnetic reluctivity term and eddy current losses through the conductivity term. The calculated magnetic and electric fields were then used to obtain frequency-dependent resistance and inductance matrices. These were combined into a complex impedance matrix that includes skin effect, proximity effect, and losses in magnetic materials.

Together with the admittance matrix obtained from the electric solver, this FEM-based approach provides a physically consistent, frequency-dependent impedance representation of the HV winding, which forms the basis for subsequent resonance analysis and insulation-condition assessment.

3. Impedance Matrix Analysis

The methodology is based on a frequency-domain, multi-conductor representation of transformer windings, where electromagnetic interactions are described by frequency-dependent impedance and admittance matrices. The impedance matrix represents series phenomena such as resistance, self- and mutual inductance, and high-frequency loss effects, while the admittance matrix captures shunt phenomena dominated by inter-turn, inter-layer, and winding-to-ground capacitances. Together, these matrices provide a compact description of how voltage and current disturbances propagate through the winding structure as a coupled electrical network.

To analyse resonance behaviour, series and shunt effects are combined into an effective total impedance matrix

$$\mathrm{Z_{tot}} = \sum_i \mathrm{Z}(\omega_i) + \mathrm{Y}^{-1}(\omega_i), \quad (5)$$

which reflects the full electromagnetic response of the winding. Resonances occur when inductive and capacitive energy storage are locally balanced, leading to sharp variations in the magnitude and structure of $\mathrm{Z_{tot}}$. Unlike terminal impedance curves, the matrix formulation preserves spatial information, allowing resonance modes to be associated with specific winding regions.

The impedance matrix also provides useful physical insight. Its diagonal terms represent the self-impedance and energy storage of each winding section, while the off-diagonal terms describe the coupling between sections. At resonance, distinct matrix patterns appear and can be related to the electrical mode shapes. These patterns indicate where voltage amplification and current concentration may occur. These regions are especially relevant for insulation and mechanical integrity, since they may be exposed to increased dielectric stress and electrodynamic forces during fast transients, such as lightning or switching impulses. Heatmaps of the real and imaginary parts for the three scenarios in Table 1 are presented in Figures 3 and 4.

By comparing impedance matrices obtained under different conditions, such as baseline versus aged states, or nominal versus mechanically displaced configurations, relative changes can be quantified using normalized difference measures

$$\Delta Z_{ij} = \frac{|Z_{ij} - Z_{ij}^{\mathrm{ref}}|}{|Z_{ij}^{\mathrm{ref}}|}. \quad (6)$$

Heatmaps of the ΔZ_{ij} for real and imaginary parts using the scenario 1 (dry – see Table 1) as the reference are shown in Figures 5 and 6. Systematic deviations in specific matrix regions provide sensitive indicators of winding deformation, insulation degradation, or changes in dielectric properties. This enables early detection of emerging faults, supports correlation between electromagnetic and mechanical resonance phenomena, and provides a physics-based foundation for resonance mitigation, insulation grading optimization, and transformer failure prevention.

4.1 Interpretation of Impedance Matrices

The imaginary part of the impedance matrix, $\mathrm{Im}\{Z\}$, reflects reactive energy storage in the winding, dominated by inductive capacitive interactions. In the dry insulation case, the matrix shows strong non uniformity and pronounced off diagonal features, indicating localized electromagnetic coupling and sharply defined resonance modes.

This behavior is characteristic of limited dielectric coupling and low inherent damping, leading to high Q resonances and localized voltage amplification within specific winding regions.

For natural ester and mineral oil, $\mathrm{Im}\{Z\}$ becomes smoother

and more homogeneous. The higher permittivity of liquid dielectrics enhances capacitive coupling between winding sections, redistributing reactive energy and suppressing strongly localized modes. As a result, resonances are broader and less severe, with reduced sensitivity to small mechanical or material variations.

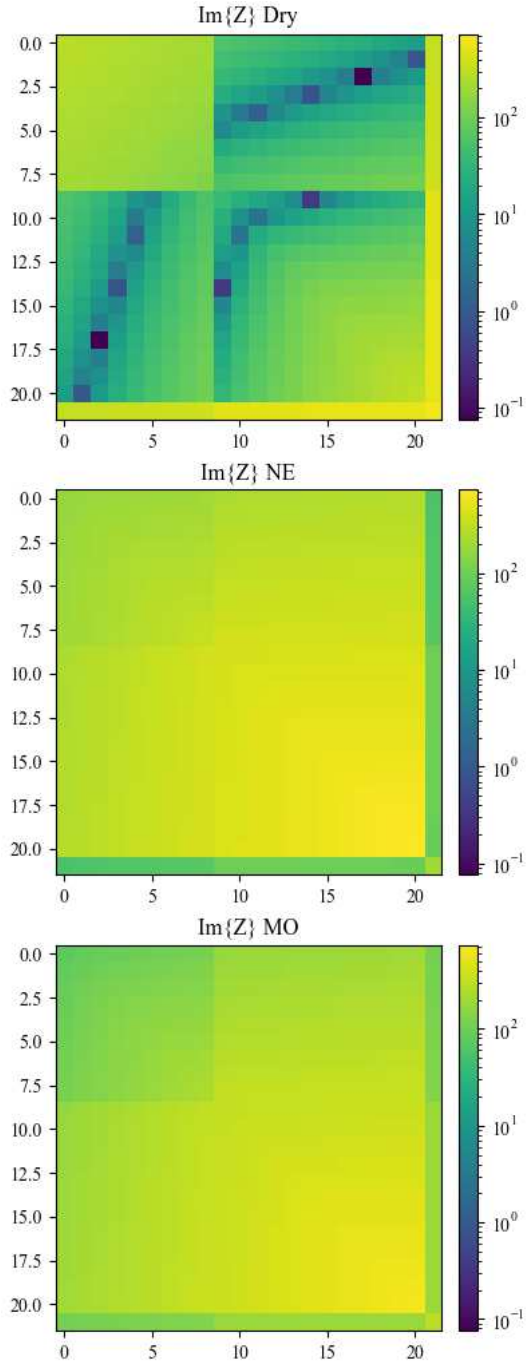


Fig. 3. Heatmap of $\mathrm{Im}\{Z_{tot}\}$ for dry, natural ester (NE), and mineral oil (MO).

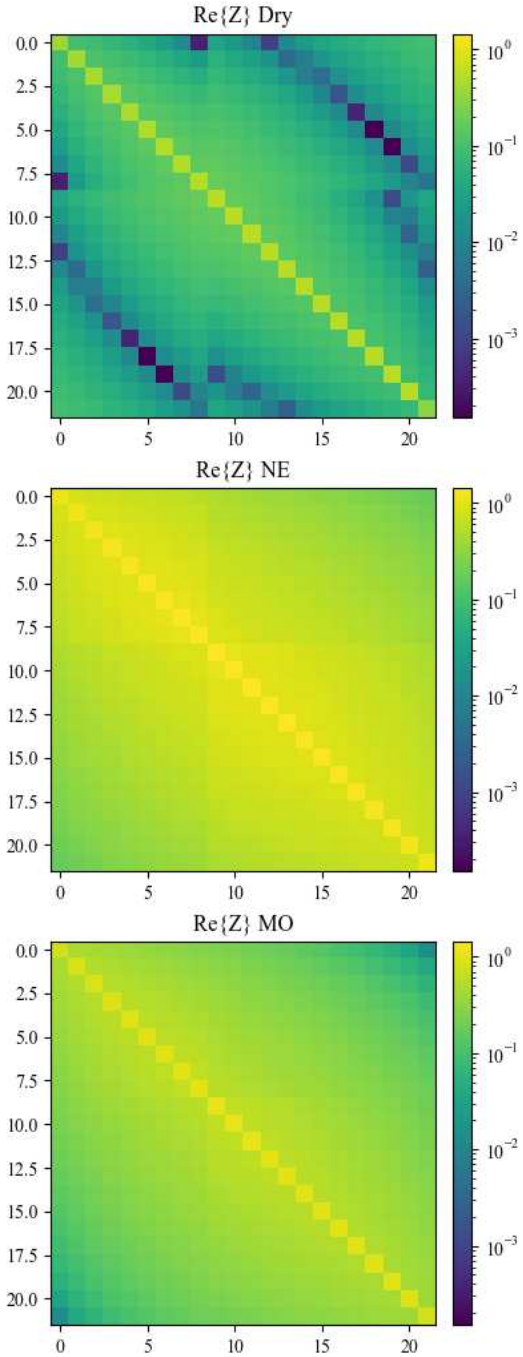


Fig. 4. Heatmap of $\mathrm{Re}\{Z_{tot}\}$ for dry, natural ester (NE), and mineral oil (MO).

The real part of the impedance matrix, $\mathrm{Re}\{Z\}$, represents energy dissipation due to conductor and dielectric losses. In the dry case, noticeable spatial variations indicate non uniform loss distribution and localized current concentration, which are associated with increased thermal and dielectric stress. In contrast, the liquid insulated cases exhibit a smooth, diagonally dominated structure, consistent with more uniformly distributed losses and effective electromagnetic damping.

Overall, the matrices indicate that dry insulation conditions promote localized, high stress resonant modes with elevated failure risk, while natural ester and mineral oil provide intrinsic damping and field homogenization. The transition from heterogeneous to smooth impedance patterns can therefore be used as a physics-based indicator of resonance severity, insulation condition, and susceptibility to winding damage under VFTO.

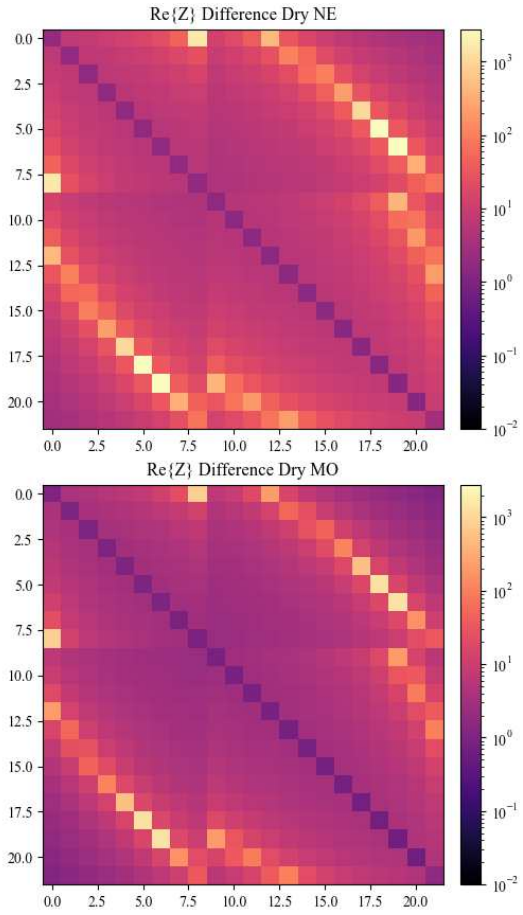


Fig. 5. Heatmaps of ΔZ_{ij} real parts. Dry is the reference, compared with NE (natural ester) and MO (mineral oil). Dark colour denotes the smallest deviations, and bright colour denotes the largest deviation to the reference.

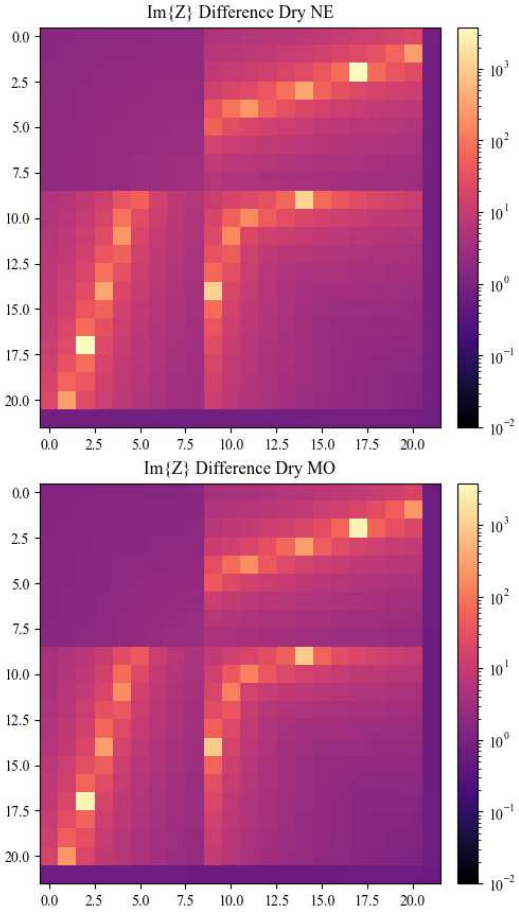


Fig. 6. Heatmaps of ΔZ_{ij} imaginary parts. Dry is the reference, compared with NE (natural ester) and MO (mineral oil). Dark colour denotes the smallest deviations, and bright colour denotes the largest deviation to the reference.

The difference matrices for the imaginary part, $\Delta\mathrm{Im}\{Z\}$, highlight how reactive energy storage changes when dry insulation is replaced by liquid dielectrics. The strongest differences appear in structured off-diagonal bands, indicating that the primary effect of ester and oil is a redistribution of inter-layer inductive–capacitive coupling rather than a uniform shift in self-impedance. These localized bands correspond to winding regions where capacitive coupling is most enhanced by the liquid dielectric, leading to a suppression of localized resonant modes present in the dry case. The similarity of the patterns for ester and oil suggests a common physical mechanism, enhanced permittivity, while differences in magnitude reflect varying degrees of resonance damping.

The real part difference matrices, $\Delta\mathrm{Re}\{Z\}$, emphasize changes in loss distribution and damping. The pronounced off diagonal deviations away from the main diagonal indicate that the introduction of liquid dielectrics alters how dissipative effects are shared between winding sections,

reducing localized loss concentrations typical of dry insulation. This redistribution implies lower peak current density and reduced thermal and mechanical stress during resonance excitation. Overall, the difference matrices provide a spatially resolved measure of how liquid insulation mitigates resonance severity, making them a sensitive indicator of both dielectric condition and susceptibility to resonance driven winding failure.

4. Frequency Response of Impedance Matrix

This methodology evaluates the transformer winding as a distributed electromagnetic network, described by frequency-dependent series impedance $Z(\omega)$ and shunt admittance $Y(\omega)$ matrices. This formulation is consistent with the physical basis of IEC 60076-18 FRA [8], where the winding is treated as an RLCG system whose frequency response reflects its electrical and mechanical integrity. By combining series and shunt paths into an effective nodal impedance matrix (see Equation (5)), the approach captures both conductive and inductive current paths as well as capacitive coupling between winding sections and to ground, which are known to dominate the FRA signature across different frequency bands.

The magnitude of each entry of $\mathrm{Z_{in}}(\omega)$, constitutes a detailed impedance frequency response of the winding. In IEC FRA terminology, low-frequency behavior is primarily governed by global inductance and resistance, mid-frequency regions are sensitive to inter-disc and inter-turn capacitances, and high-frequency regions reflect local winding geometry and dielectric properties. Resonances and anti-resonances arise when effective inductive L_{eq} and capacitive C_{eq} elements satisfy

$$\omega_r \approx \frac{1}{\sqrt{L_{\mathrm{eq}} C_{\mathrm{eq}}}} \tag{7}$$

producing characteristic winding fingerprint. Changes in these features correspond to variations in electromagnetic coupling, capacitance distribution, or damping, which are the same physical mechanisms exploited in FRA for detecting mechanical displacement and insulation degradation. Different insulation systems modify the shunt admittance matrix through changes in permittivity and dielectric losses, i.e.:

$$\mathbf{Y}(\omega) = \mathbf{G}(\omega) + j\omega\mathbf{C}. \tag{8}$$

An increase in effective permittivity shifts resonances toward lower frequencies, while higher dielectric losses increase damping and reduce resonance sharpness. From an IEC FRA perspective, such effects manifest as systematic shifts or amplitude changes in specific frequency bands, enabling discrimination between insulation-related effects and purely mechanical winding movements. The matrix-based formulation further extends conventional terminal FRA by revealing mutual impedance terms between winding sections, which are particularly sensitive to localized insulation weaknesses or inter-disc spacing changes that may not be evident in a single transfer function.

By providing a physics-based impedance spectrum over a wide frequency range, the method supports both diagnostic assessment and robust winding design. In service, deviations from a reference response can be interpreted using IEC FRA rules for frequency-band sensitivity, while in design studies the influence of insulation media and winding layout on resonance locations and damping can be quantified. This directly addresses one of the key IEC FRA objectives: linking observed frequency-response changes to specific physical causes within the winding structure.

Figure 7 presents the magnitude of the frequency-dependent effective impedance matrix of a transformer winding, evaluated for three different insulation scenarios. For each case, the impedance response is shown over the frequency range from DC to 20 kHz. Each subplot corresponds to one insulation system, while the multiple curves within each subplot represent the magnitudes of the individual entries of the effective impedance matrix, including both self and mutual impedance terms between winding sections The impedance magnitude $\mathrm{S}(\omega)$ is expressed in decibels and plotted as a function of frequency:

$$\mathbf{S}(\omega) = 20\log10\left|\mathrm{Z}_{in,ij}(\omega)\right| \tag{9}$$

This representation captures the distributed electromagnetic behavior of the winding, highlighting resonances and anti-resonances associated with the interaction of inductive and capacitive elements. The comparison across insulation systems allows the influence of dielectric properties on the overall frequency response of the winding to be directly assessed within an IEC FRA-consistent framework.

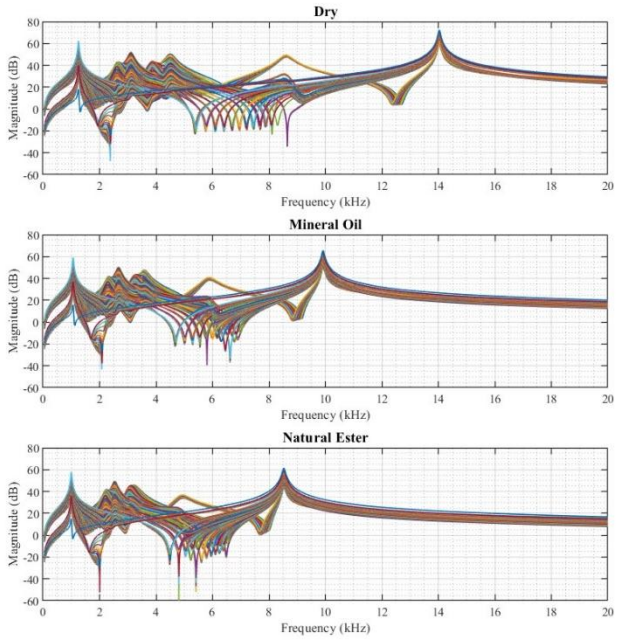


Fig. 7. Frequency response S(ω) of the 3 different insulator systems.

4.2 Interpretation of Impedance Matrices

The impedance frequency responses exhibit the characteristic multi resonant behavior of transformer windings described in IEC FRA, reflecting the interaction between distributed inductances and capacitances along the winding. In the low frequency range, the three insulation cases show comparable behavior, indicating that the global inductive properties of the winding are largely unaffected by the dielectric medium. In contrast, the mid frequency range reveals pronounced resonances and anti resonances, which are highly sensitive to inter disc and inter turn capacitances. Here, the dry insulation case shows sharper resonances and a wider space between impedance curves, indicating weak damping and non uniform electrical coupling between winding sections.

The introduction of liquid insulation significantly modifies the response. Both mineral oil and natural ester shift resonant frequencies toward lower values, consistent with increased effective permittivity, while simultaneously reducing resonance sharpness due to higher dielectric losses. Among the tested cases, natural ester insulation shows the most damped response and the narrowest dispersion of impedance magnitudes, suggesting a more homogeneous voltage distribution along the winding. From an FRA perspective, these differences suggest changes in shunt admittance rather than mechanical deformation, underlining the importance of insulation properties at mid and high frequencies.

Sharp and weakly damped resonances – as observed in the dry insulation case – can lead to significant internal voltage amplification and localized insulation stress, even when terminal voltages remain within test limits. The smoother and more damped responses obtained with mineral oil and especially natural ester simply reduced susceptibility to internal overvoltages during impulse testing, providing a clear frequency domain explanation for the improved impulse withstand behaviour commonly associated with liquidinsulated windings. domain explanation for the improved impulse withstand insulated windings.

5. Summary and Conclusion

This work presented a physics-based methodology for analyzing transformer winding resonance behavior through FEM-derived, frequency-dependent impedance matrices, with particular emphasis on the influence of insulation systems. A 630kVA transformer HV layer-wound winding was modeled under dry, mineral-oil, and natural-ester insulation conditions. By combining electro- and magneto-quasistatic FEM formulations, impedance and admittance matrices were extracted that consistently capture inductive coupling, capacitive effects, dielectric losses, and frequency-dependent material behavior. The matrix-based formulation preserves spatial information that is not accessible from terminal measurements alone, enabling resonance modes to be linked directly to specific winding regions and insulation configurations.

The results demonstrate that insulation properties play a dominant role in shaping winding resonance characteristics. Dry insulation promotes strongly localized, weakly damped resonant modes, leading to elevated internal voltage amplification and higher susceptibility to dielectric and mechanical stress under VFTO. In contrast, mineral oil and natural ester enhance capacitive coupling and introduce distributed dielectric damping, resulting in smoother impedance matrices, reduced resonance sharpness, and more homogeneous voltage distribution. The comparison of impedance matrices and their frequency responses provide a clear electromagnetic explanation for the improved impulse withstand behavior of liquid-insulated windings. Overall, the proposed methodology extends conventional FRA interpretation by offering a spatially resolved, physics-based framework that supports both transformer design optimization and early detection of insulation-related degradation and resonance-driven failure mechanisms.

References

[1] CIGRE WG C4.45, Measuring techniques and characteristics of fast and very fast transient overvoltages in substations and converter stations (TB 836), 2021.

[2] M. Popov, “General approach for accurate resonance analysis in transformer windings,” Electric Power Systems Research, vol. 161, pp. 45–51, 2018.

[3] D. L. Álvarez, J. A. Rosero, E. E. Mombello, “Analysis of Impedance Matrix in Transformer Windings through the Finite Element Method (FEM),” IEEE TDC LA, 2014.

[4] B. Jurišić, L. Bučar, I. Uglešić, “Calculation of voltage distribution along the transformer winding using the wide band transformer model,” Journal of Energy, vol. 66, 2017.

[5] R. Haller, V. Kotlán, “Transient behavior of line connections between GIS and transformers,” ISH Collection, 2017.

[6] Dennis Albert, Power transformer diagnostics and DC bias (FRA overview), CIGRE A2 Webinar Deck, June 26, 2024.

[7] D. J. Wilcox, W. G. Hurley, M. Conlon, “Calculation of self and mutual impedances between sections of transformer coils,” IEE Proc. C, vol. 136, no. 5, pp. 308–314, 1989.

[8] IEC 60076-18, Power transformers – Part 18: Measurement of frequency response, International Electrotechnical Commission (IEC), Geneva, Switzerland.

[9] E. Rahimpour, J. Christian, K. Feser and H. Mohseni, “Transfer Function Method to Diagnose Axial Displacement and Radial Deformation of Transformer Windings”, IEEE Transactions on Power Delivery, Vol.18, No.2, pp. 493-505, April 2003

[10] E. Rahimpour, M. Jabbari and S. Tenbohlen, “Mathematical Comparison Methods to Assess Transfer Functions of Transformers to Detect Different Types of Mechanical Faults”, IEEE Transactions on Power Delivery, Vol.25, No.4, pp. 2544-2555, October 2010